Discovery and structural characterization of a small molecule 14-3-3 protein-protein interaction inhibitor

Jing Zhao[a,b,1], Yuhong Du[a,c,1], John R. Horton[d,1], Anup K. Upadhyay[d,1], Bin Lou[a], Yan Bai[a], Xing Zhang[d], Lupei Du[e], Minyong Li[e], Binghe Wang[e], Lixin Zhang[a,f], Joseph T. Barbieri[g], Fadlo R. Khuri[h], Xiaodong Cheng[d,2], and Haian Fu[a,h,c,2]

[a]Departments of Pharmacology; [d]Biochemistry; and [h]Hematology and Medical Oncology; [c]Emory Chemical Biology Discovery Center, Emory University School of Medicine, Atlanta, GA 30322; [b]Department of Biochemistry and Molecular Biology, the Fourth Military Medical University, 17 Changle West Road, Xi'an 710032, China; [e]Department of Chemistry, Georgia State University, Atlanta, GA 30302; [f]Institute of Microbiology, Chinese Academy of Sciences, Beijing 100101, China; and [g]Department of Microbiology and Molecular Genetics, Medical College of Wisconsin, Milwaukee, WI 53226

Edited by Tony Pawson, Samuel Lunenfeld Research Institute, Toronto, Canada, and approved July 27, 2011 (received for review January 1, 2011)

The 14-3-3 family of phosphoserine/threonine-recognition proteins engage multiple nodes in signaling networks that control diverse physiological and pathophysiological functions and have emerged as promising therapeutic targets for such diseases as cancer and neurodegenerative disorders. Thus, small molecule modulators of 14-3-3 are much needed agents for chemical biology investigations and therapeutic development. To analyze 14-3-3 function and modulate its activity, we conducted a chemical screen and identified 4-[(2Z)-2-[4-formyl-6-methyl-5-oxo-3-(phosphonatooxymethyl)pyridin-2-ylidene]hydrazinyl]benzoate as a 14-3-3 inhibitor, which we termed FOBISIN (FOurteen-three-three BInding Small molecule INhibitor) 101. FOBISIN101 effectively blocked the binding of 14-3-3 with Raf-1 and proline-rich AKT substrate, 40 kD_a and neutralized the ability of 14-3-3 to activate exoenzyme S ADP-ribosyltransferase. To provide a mechanistic basis for 14-3-3 inhibition, the crystal structure of 14-3-3ζ in complex with FOBISIN101 was solved. Unexpectedly, the double bond linking the pyridoxal-phosphate and benzoate moieties was reduced by X-rays to create a covalent linkage of the pyridoxal-phosphate moiety to lysine 120 in the binding groove of 14-3-3, leading to persistent 14-3-3 inactivation. We suggest that FOBISIN101-like molecules could be developed as an entirely unique class of 14-3-3 inhibitors, which may serve as radiation-triggered therapeutic agents for the treatment of 14-3-3-mediated diseases, such as cancer.

small molecule 14-3-3 modulator

Initially discovered as a protein abundant in the brain, the 14-3-3 family of proteins consists of seven defined isoforms (β, ϵ, γ, η, σ, τ, and ζ) in mammals and is widely expressed in all tissues and organs examined (1–3). 14-3-3 acts as an adaptor protein that controls the function of its target proteins through highly regulated protein–protein interactions. Studies on the interaction of 14-3-3 with phosphorylated Raf-1 led to the discovery of 14-3-3 as the founding member of the class of phosphoserine/threonine-binding protein modules (4–8). Reversible phosphorylation of target proteins at a defined motif dictates the 14-3-3 association in response to dynamic actions of cellular kinases and phosphatases. These 14-3-3 recognition motifs include the prototype sequence, RSxpS/TxP (mode 1), and RxxxpS/TxP (mode 2), pS/TX-COOH (mode 3), where x stands for any amino acid (8–11). The availability of well characterized 14-3-3 recognition motifs coupled with advanced genomics, proteomics, and functional biology approaches has revealed an entirely new landscape in which 14-3-3 binds a variety of signaling molecules, controlling their function in response to environmental signals (8, 9, 12–14). More than 200 ligand proteins have been identified for 14-3-3 (12). Depending on the nature of its target proteins, 14-3-3 binding impacts multiple signaling pathways that determine cell fate and organ development. For example, 14-3-3 association controls Raf signaling fidelity, neutralizes Bad-mediated apoptosis, and couples histone H3 with H4 to create a histone code for transcriptional elongation (2, 3, 15). Through these highly regulated interactions, 14-3-3 proteins govern diverse physiological processes as well as a wide range of pathophysiological events. For example, dysregulated 14-3-3 signaling contributes to the development of a number of human diseases, such as cancer and neurodegenerative diseases (1–3). Thus, 14-3-3 proteins are promising molecular targets for probe discovery and therapeutic development.

In an effort to discover 14-3-3 protein–protein interaction modulators, we have previously reported the development and structural characterization of peptide 14-3-3 antagonists, R18 and difopein (16–18), which have been widely used in the field to manipulate 14-3-3/client protein interactions for functional studies. It is expected that small molecule 14-3-3 modulator discovery would provide added advantages to rapidly advance the 14-3-3 field, which impacts a wide range of biomedical areas. Here we report our experimental chemical screening effort, the identification and analysis of FOBISIN101 as a phosphoSer/Thr-mimetic agent, and the structural details of the FOBISIN101/14-3-3ζ interaction. This study revealed an unexpected covalent modification of 14-3-3ζ by a FOBISIN 101 derivative at a critical ligand binding site, Lys120, explaining its potent 14-3-3 inhibitory effect.

Results and Discussion

Using a fluorescence polarization-based 14-3-3 binding assay (19), we screened the LOPAC library for compounds that disrupt the interaction of 14-3-3γ with the pS259-Raf-1 peptide and identified FOBISIN101 (**F1** in Fig. 1*A*) as a potential 14-3-3 inhibitor (Fig. S1) (19, 20). **F1** consists of a pyridoxal-phosphate moiety linked to p-amino-benzoate via an N = N bond. Because the screening assay utilized a 14-3-3-binding peptide, it is essential to demonstrate that FOBISIN101 is capable of disrupting the interaction of 14-3-3 with its full-length binding proteins. We employed three complementary biochemical and functional assays for this purpose. A Glutathione S-transferase (GST) fusion 14-3-3 affinity chromatography assay was used to examine the ability of **F1** to disrupt the 14-3-3 association with two well established partners, Raf-1 and proline-rich AKT substrate, 40 kD_a (PRAS40). The addition of increasing concentrations of **F1** to the cell lysates led to a dose-dependent release of PRAS40 and Raf-1, supporting an effective inhibitory role of **F1**. This inhibi-

Author contributions: Y.D., F.R.K., X.C., and H.F. designed research; J.Z., Y.D., J.R.H., A.K.U., B.L., Y.B., and X.Z. performed research; B.L., L.D., M.L., B.W., L.Z., and J.T.B. contributed new reagents/analytic tools; J.Z., Y.D., J.R.H., A.K.U., Y.B., X.Z., L.Z., F.R.K., X.C., and H.F. analyzed data; and J.Z., Y.D., J.R.H., A.K.U., X.C., and H.F. wrote the paper.

The authors declare no conflict of interest.

This article is a PNAS Direct Submission.

Data deposition: The atomic coordinates have been deposited in the Protein Data Bank, www.pdb.org (PDB ID code 3RDH).

[1]J.Z., Y.D., J.R.H., A.K.U. contributed equally to this work.

[2]To whom correspondence may be addressed. E-mail: hfu@emory.edu or xcheng@emory.edu.

This article contains supporting information online at www.pnas.org/lookup/suppl/doi:10.1073/pnas.1100012108/-/DCSupplemental.

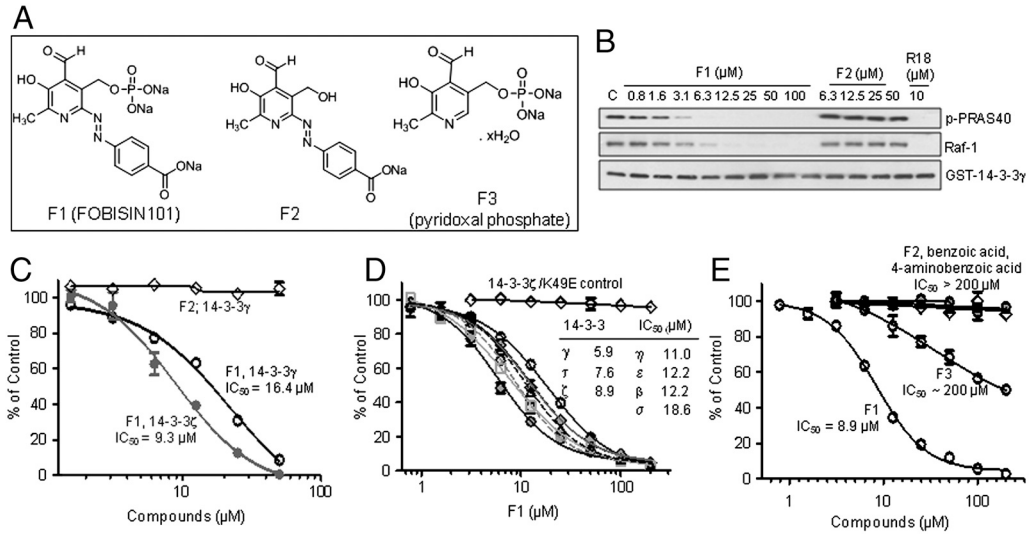

Fig. 1. Discovery of FOBISIN (*A*) Chemical structures of FOBISIN 101 (F1), F2 (dephosphorylated F1), and F3 (pyridoxal-phosphate). (*B*) F1 blocks the binding of 14-3-3 to full-length Raf-1 and PRAS40 in cell lysates. GST-14-3-3γ was mixed with COS-7 cell lysate in the presence of test compounds. The 14-3-3γ complex was isolated by GST-pull-down. The presence of Raf-1 and PRAS40 in the 14-3-3γ complex was revealed by Western blot analysis. (*C*) Inhibition of the interaction between PRAS40 and 14-3-3γ or 14-3-3ζ by **F1** in an ELISA assay. Interaction of PRAS40 with GST-14-3-3γ or 14-3-3ζ immobilized on an anti-GST antibody-coated plate gave rise to robust ELISA signals as detected by anti-PRAS40 antibody. (*D*) F1 inhibits ExoS activation by all seven isoforms of 14-3-3. ExoS and its substrates were incubated with 14-3-3 proteins in the presence or absence of F1. 14-3-3-dependent ExoS enzymatic activity was quantified by the amount of ^{32}P-ADP-ribose incorporated into SBTI, % control relative to samples without F1 was calculated. (*E*) Dephosphorylated F1 (F2) does not affect 14-3-3-mediated ExoS activity in an ExoS assay as described in (*D*). The results in *c* – *e* were presented as means ± SD ($n = 3$) of one representative experiment. The experiments were repeated at least three times with similar results.

tion occurred in a manner similar to the action of a defined 14-3-3 antagonist peptide, R18 (17) (Fig. 1*B*). **F1** appears to be a pan-14-3-3 inhibitor as it decreased the binding of Raf-1 to all seven 14-3-3 isoforms in a dose-dependent manner (Fig. S2). A quantitative enzyme-linked immunosorbent assay established a half-maximal inhibitory concentration (IC_{50}) for **F1**, which was 9.3 or 16.4 μM, respectively, for the binding of 14-3-3ζ or 14-3-3γ to PRAS40 (Fig. 1*C*). Furthermore, **F1** effectively blocked the ability of all seven 14-3-3 isoforms to stimulate exoenzyme S (ExoS) ADP-ribosyltransferase (IC_{50} = 6–19 μM) in a functional assay (21) (Fig. 1*D*). Because ExoS is a nonphosphorylated client protein, **F1** is capable of interfering with the binding of both phosphorylated and nonphosphorylated client proteins to 14-3-3. Together, these data suggest a direct action of **F1** on 14-3-3 proteins.

To provide a structural explanation for the inhibitory effect of **F1** on 14-3-3 proteins, **c**ompound **F1** was soaked into preformed crystals of 14-3-3ζ. These cocrystals were bright orange in color (Fig. 2*A*). During the X-ray data collection, immediately after exposure to synchrotron radiation, the cocrystals turned brownish, then yellow, and eventually became colorless. We determined the complex structure to a resolution of 2.39 Å (Table S1). The crystal contains four monomers (two dimers) within the asymmetric unit (Fig. 2*B*), with a root-mean-square-deviation of <0.5 Å of 230 pairs of Cα atoms between the monomers. Each monomer consists of nine α helices that form an a mphipathic groove where a client protein is located (9, 22–24). **F1** is bound to the basic surface of the peptide-binding groove of each monomer. However, only the pyridoxal-phosphate moiety of **F1** was found in this groove (Fig. 2*C*). The **F1** exocyclic nitrogen atom formed a covalent bond with the side chain terminal nitrogen of Lys120, forming a diazene adduct with a N-N distance of approximately 1.2 Å. The **F1** phosphate group interacts with the side chain of Lys49 and Asn173, while one face of the pyridoxal ring makes van der Walls contact with the side chain of Ile217 (Fig. 2*D*, Fig. S3). These interactions position the **F1** derivative in a defined conformation. In addition, a solvent molecule bridges Arg56 and Arg127.

We superimposed the **F1**-bound structure of 14-3-3ζ to that of 14-3-3 bound to either the pS259-Raf-1 (PDB 3CU8) or pS10-histone H3 (25) (PDB 2C1N) peptide. In order to interact with phosphorylated ligands, 14-3-3ζ engages a cluster of basic or polar residues, including (*i*) Arg56, Arg127, and Tyr128, which coordinates the binding of the phosphate group (Fig. 2*E*) and (*ii*) Asn173, whose side chain oxygen atom forms a hydrogen bond with the main chain amide nitrogen of the residue C-terminal to the phosphoserine and involves an intramolecular interaction network forming a hydrogen bond with Asp114, which in turn forms a salt bridge with Lys120 (Fig. 2*F*). The conformation of peptide residues at +2 and beyond differs when the peptide exits from the 14-3-3 ligand binding groove, with Raf-1 to the left and histone H3 to the right of Lys49, as shown in Fig. 2*E*.

It appears as though the phosphate group of covalently linked **F1** shifted approximately 4 Å away from the phosphoserine binding site, towards Lys120 (Fig. 2*G*). Mutagenesis of 14-3-3ζ coupled with direct binding studies using isothermal titration calorimetry indicated the importance of R56 and R60 in the binding of native uncleaved **F1** (Fig. S4, Table S2), which supports the proposed model in Fig. 2. We reasoned that the phosphate moiety of **F1** might be critical for its inhibitory activity by mimicking the phosphorylated peptide motif for 14-3-3 binding. We thus generated the compound **F2**, which lacks the phosphate group, and observed that this compound had a drastically reduced effect in blocking 14-3-3 binding to Raf-1 or PRAS40 (Fig. 1 *B* and *C*, Fig. S2) and in inhibiting 14-3-3-mediated activation of ExoS (Fig. 1*E*). Moreover, changes in the phenyl ring structure also showed some effect on the 14-3-3/Raf-1 interaction (Fig. S5), demonstrating the involvement of the azophenyl substructure in 14-3-3 interaction. These data support **F1** as a 14-3-3 inhibitor and highlight its phosphate moiety as a primary functional component. We modeled intact **F1** by superimposing the **F1** phosphate group onto that of phosphoserine and rotating the torsion angles to reach maximum overlap with the bound peptide (Fig. 3*A*). The model suggests that the side of the pyridoxal ring with the phosphate group superimposes well with peptide backbones before and after phosphoserine, while the benzoate ring

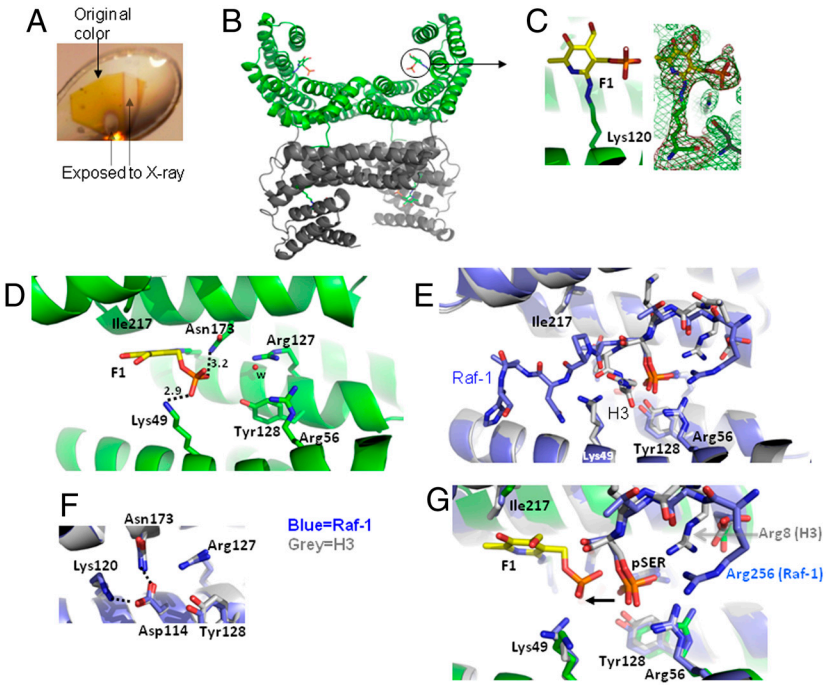

Fig. 2. Structure of the 14-3-3ζ/F1 fragment covalent complex (*A*) Example color change of the 14-3-3ζ/F1 crystal after exposure to X-rays. (*B*) Two dimers of 14-3-3ζ in the asymmetric unit. (*C*) Covalently modified Lys120 in the peptide-binding groove of 14-3-3ζ. Omit electron densities, Fo-Fc (red mesh) and 2Fo-Fc (green mesh), contoured at 4σ and 1.2σ above the mean, respectively, are shown for F1-modified Lys120. (*D*) Details of 14-3-3ζ and F1 fragment interactions. The letter w indicates a solvent [either water in molecule (*A-C*) or a partially occupied phosphate in molecule (*D*)]. (*E*) Superimposition of 14-3-3ζ in complex with a Raf-1 peptide (blue) (PDB 3CU8) and a histone H3 peptide (gray) (PDB 2C1N). For clarity, H3 residues 12–14 (which point toward the viewer) were removed. (*F*) Lys120 is involved in intramolecular interactions. (*G*) Superimposition of a covalently bound F1 fragment (yellow) with that of Raf-1 (blue) and H3 (gray) phosphoserine peptides.

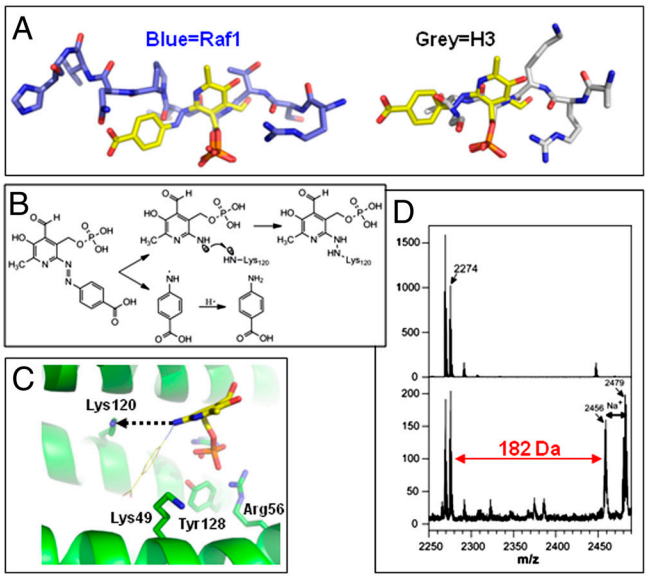

Fig. 3. Model of intact F1 bound to 14-3-3ζ (*A*) Superimposition of the pyridoxal-phosphate moiety and the phosphoserine of a Raf-1 peptide (left) or histone H3 peptide (right). For clarity, H3 residues 13-14 (which point toward the viewer) were removed. (*B*) Proposed bond-breaking and bond-making process. (*C*) Lys120 lies in a position for a preferred attack trajectory. (*D*) Mass spectrum profiles (in the reflection mode of acquisition of the spectrum) showing a 14-3-3ζ fragment containing Lys120 digested from crystals with (bottom) and without (top) exposure to X-rays. The addition of 182 Da corresponds to modification of Lys120 (262 Da) with the loss of a phosphate group (HPO_3) from the peptide (by a reduction of 80 Da in the mass), presumably due to laser (337 nm) induced metastable decomposition during the MALDI ionization process (35–38).

could point to the peptide exit pathway similar to that of Raf-1 (Fig. 3*A*, left box).

To explore the possible cause of the covalent modification of 14-3-3 by **F1**, we hypothesized that radiation exposure cleaves the N = N diazene bond thereby releasing the paraaminobenzoic acid moiety into the solvent, while the hydrogen binding interaction holds the pyridoxal-phosphate moiety in place within the 14-3-3 binding site (Fig. 3*B*). In this model, the reactive nitrogen of the pyridoxal-phosphate group is approximately 6–7 Å from either Lys120 or Lys49, respectively (Fig. 3*C*). However, the side chain Nϵ of Lys120 is roughly parallel, while that of Lys49 is roughly perpendicular, to the plane of the pyridoxal ring. We suggest that bond-breaking and bond-making processes proceed through specific attack trajectories. The preferred attack trajectory might be the one which lies parallel to the plane of the ring and facilitates the formation of a new nitrogen bond of the cleaved compound with the side chain of Lys120, leading to covalent modification and inactivation of 14-3-3 function. Indeed, mutating Lys120 to Glu alone is sufficient to inactivate 14-3-3ζ (Fig. S6).

The N = N bond in diazene compounds is generally sensitive to radiation and is known to undergo photolysis to generate reactive organic radicals (26). We note that another plausible source of the covalent adduct is through imine (Schiff base) formation between the ϵ-amino group of a lysine and the aldehyde group (with the loss of water) on the pyridoxal-phosphate portion of the inhibitor. However, three lines of evidence argue against this possibility. First, the electron density is of sufficient quality to identify the phosphate group, its associated pyridine ring, and the aldehyde (with a two bond length -C = O away from a ring atom). If the site of covalent attachment is via imine formation, irradiation-induced cleavage of the N = N bond would be reduced to NH_2 (in this case, one bond length away from a ring atom). Second, the covalent adduct is only formed after exposure

to X-rays. It is not known whether imine formation with pyridoxal-phosphate requires photolysis. Gel digestion and mass spectrometric analysis of digested peptides obtained from **F1**-soaked crystals that were not exposed to X-rays showed no adduct peak (Fig. 3*D*, top box). Importantly, only the X-ray-treated samples showed a mass addition corresponding to a peptide fragment of residues 114-131 with modified Lys120 (Fig. 3*D*, bottom box). Therefore, the fragmentation and covalent adduct formation of **F1** observed in the 14-3-3ζ crystal structure very well could be induced by X-ray radiation during data collection, as evident by the change of color (Fig. 2*A*). Third, assuming the site of covalent attachment is via imine formation and the pyridine ring takes on the same conformation (by flipping the ring 180° horizontally as shown in Fig. 2*C*), the paraaminobenzoic acid moiety would point to the solvent without any specific contact to the protein. However, the pyridoxal-phosphate (F3 in Fig. 1*A*) has much reduced potency (Fig. 1*E*), indicating that the phenyl ring structure still contributes to the inhibitory activity of **F1**, which is supported by data in Fig. S5.

In conclusion, we have identified and experimentally confirmed a series of small molecule phospho-binding site inhibitor and revealed structural details of one such molecule with 14-3-3ζ. Because of the specificity of the mode of binding as revealed by the cocrystal structural studies and the potent effect on both phosphorylated and nonphosphorylated client protein binding to 14-3-3 proteins, this pyridoxal-phosphate class of compounds are expected to define a unique class of 14-3-3 inhibitors for physiological and therapeutic investigations. It is important to note that the **F1** class of compounds have been investigated as ionotropic P2X receptor antagonists (20). Rich medicinal chemistry information around this structural scaffold will greatly facilitate their development as 14-3-3 modulators. Importantly, we also offer a prodrug concept for 14-3-3-mediated diseases. For example, **F1**-like molecules could be developed as radiation-triggered therapeutic agents for the treatment of cancer. It is envisioned that such 14-3-3 inhibitors alone may show negligible toxicity to the host; however, radiation therapy targeted to a particular tumor area may specifically cleave such designed 14-3-3 inhibitors and lead to their covalent modification and potent inactivation of 14-3-3 proteins in tumors.

Materials and Methods

Molecular and Cell Biology Reagents. The expression vectors for GST-14-3-3 and His-14-3-3 isoforms were constructed as previously described (27). Glutathione agarose beads and nickel-affinity columns were purchased from GE Healthcare. Anti-Raf-1 and anti-GST antibodies were from Santa Cruz and the anti-PRAS40 antibody was from Biosource. 14-3-3ζ was expressed in *Escherichia coli* BL21(DE3) harboring pET-15b-derived plasmids and purified using Ni^{2+} chelating chromatography essentially as described (21). Hexahistidine tags were removed by thrombin digestion. The 14-3-3 protein used for crystallization was further purified by gel filtration chromatography (Superdex 200 in a Pharmacia FPLC system). ExoS was purified as previously described (28). The LOPAC library was purchased from Sigma-Aldrich. COS-7 cells were grown in DMEM supplemented with 10% FBS.

Florescence Polarization Assay and Chemical Screening. The 14-3-3 FP assay was carried out in black 384-well microplates in a total volume of 50 μL (19). Assay reaction buffer (49 μL: 1 μM GST-14-3-3γ and 2 nM TMR-pS259-Raf peptide in Hepes buffer) was dispensed to each well. Test compound (1 μL of 2 mM stock in DMSO) was added to the reaction buffer using a Sciclone liquid handler (Caliper LifeSciences). Plates were incubated at room temperature and the FP value in millipolarization (mP) units was recorded with an Analyst HT reader (Molecular Devices). An excitation filter at 545 nm and an emission filter at 610 to 675 nm were used with a dichroic mirror at 565 nm. Data analysis was conducted using CambridgeSoft software. Compounds with recorded mP values less than three standard deviation from the negative controls were considered positive hits.

Enzyme-Linked Immunosorbent Assay. The 14-3-3 ELISA assay was developed in 96-well microplates coated with either anti-GST antibody or glutathione (Pierce Biotechnology). This assay monitors the interaction of recombinant GST-tagged 14-3-3 proteins with endogenous client proteins, such as PRAS40, in COS-7 cell lysate. Briefly, GST-14-3-3 protein (1 μM) immobilized on an anti-GST plate was incubated with a test compound before adding COS-7 cell lysates in 1% NP-40 lysis buffer (16). After incubation and washing, antibodies specific to PRAS40 along with peroxidase-labeled anti-rabbit IgG (50 μL; 1:1,000 dilution) were added. After washing, 100 μL of tetramethylbenzidine was added. The reaction was stopped with sulfuric acid (0.1 N) and recorded at 450 nm on an Envision™ reader (Perkin Elmer). IC_{50} values were calculated using GraphPad software.

GST Pull-Down Assay and Western Blotting. For binding assays, GST-14-3-3 proteins (1 μg) were preincubated with various concentrations of test compound before COS-7 cell lysates were added. Client proteins associated with GST-14-3-3 were captured by glutathione Sepharose beads while unbound proteins were removed by washing (1% NP-40 buffer). The fraction that was bound to the beads was analyzed by SDS-PAGE followed by immunoblotting with antibodies specific to Raf-1, PRAS40, and GST.

ExoS Activation Assay. To examine the functional effect of test compounds on 14-3-3 proteins, we utilized the 14-3-3-dependent ExoS ADP-ribosyltransferase assay (21). This assay is used as a functional readout for 14-3-3 inhibitors. Briefly, 14-3-3 protein was preincubated with test compounds, followed by incubation with ExoS in the presence of substrates (SBTI, NAD, and 0.35 μCi of [adenylate-^{32}P]NAD^+ as a reaction tracer). The reaction was terminated by spotting assay mixture onto P81 phosphocellulose paper (Whatman). After washing, radioactivity incorporated into SBTI by ExoS was determined by liquid scintillation counting. Enzyme activities were expressed as picomoles of ADP-ribose incorporated per min per microgram of ExoS. The inhibitory effect of compounds was expressed as percent inhibition of ExoS activity over vehicle control.

Chemical Synthesis of Compound F2. A 5.1 mg sample of **F1** was dissolved in 1.0 mL of hydrofluoric acid (48%, Sigma-Aldrich) and incubated in an ice bath for 2 h. The solution was adjusted to a pH of 5 using a saturated NaOH aqueous solution. The solution was dried under a vacuum using a rotary-evaporator at 30 °C. Precooled (−20 °C) ethanol was added to the remaining residue. The solid residue was filtered and the filtrate was dried to give 3.1 mg of a brown solid product. Yield: 89%.

ESI-NEG: [M-H] 314.1

^{1}H-NMR (400 MHz, CD_3OD): 8.02–8.24 (d, 4H), 6.30 (m, 1H), 5.35–5.38 (m, 2H), 2.63 (s, 3H).

Crystallography. The 14-3-3ζ protein (10 mg/mL in 20 mM Tris/HCl, pH 8.5, 100 mM NaCl) was crystallized by the hanging drop vapor diffusion method using conditions similar to those previously described (22) (25% PEG3350, 100 mM Tris-HCl, pH 8.5, 10 mM $MgCl_2$, 1 mM $NiCl_2$, 1% glycerol at 16 °C). The 14-3-3ζ crystals were soaked with 5 mM **F1** compound for 3 d. The crystals were then momentarily immersed into well solution containing either 25% ethylene glycol or glycerol as a cryoprotectorant and frozen by plunging into liquid nitrogen. The crystals were then stored in a liquid nitrogen dewar until data collection at the SET-CAT synchrotron beamline at the Advanced Photon Source of Argonne National Laboratory. Structural determination of the 14-3-3ζ/**F1** complex proceeded by molecular replacement with the program PHASER (29) using the 14-3-3 coordinates of a 14-3-3/ExoS complex (PDB 2O02) (30). Refinement of the model proceeded with manual manipulation using the graphic programs COOT (31) and O (32) and computational manipulation with the program CNS (33). On the basis of evident electron density, we modeled the F1 modified Lys120, whose topology and parameter files for refinement were obtained from the Dundee PRODRG2 Server (34) (http://davapc1.bioch.dundee.ac.uk/prodrg/).

Mass Spectrometry. Covalent adduct formation between 14-3-3ζ-K120 and fragmented **F1** was verified by performing MALDI-TOF-MS analysis of V8-protease (New England BioLab) digested peptide fragments of the F1-protein crystals with or without X-ray exposure.

Detailed information on mass spectrometry, isothermal titration calorimetry, mutagenesis analysis is included in the *SI Materials and Methods* as well as additional information on FOBISIN 104–107.

ACKNOWLEDGMENTS. We thank Paul R. Thompson for critical comments. The Department of Biochemistry at the Emory University School of Medicine supported the use of the SER-CAT synchrotron beamline at the Advanced Photon Source of Argonne National Laboratory, local X-ray facility and MALDI-TOF mass spectrometry and HTS was performed at the Emory Chemical Biology Discovery Center. This work was supported in part by the National Institutes

of Health Grants P01 CA116676 (to F.R.K and H.F.), GM068680 and GM092035 (to X.C.), AI030162 (to J.T.B.), Georgia Cancer Coalition (to F.R.K. and H.F.), Georgia Research Alliance (to X.C. and H.F.), and Chinese Academy of Sciences K. C. Wong Awards (to L.Z. and H.F.).

1. Aitken A (2006) 14-3-3 proteins: a historic overview. *Semin Cancer Biol* 16:162–172.
2. Dougherty MK, Morrison DK (2004) Unlocking the code of 14-3-3. *J Cell Sci* 117:1875–1884.
3. Fu H, Subramanian RR, Masters SC (2000) 14-3-3 proteins: structure, function, and regulation. *Annu Rev Pharmacol Toxicol* 40:617–647.
4. Fantl WJ, et al. (1994) Activation of Raf-1 by 14-3-3 proteins. *Nature* 371:612–614.
5. Fu H, et al. (1994) Interaction of the protein kinase Raf-1 with 14-3-3 proteins. *Science* 266:126–129.
6. Irie K, et al. (1994) Stimulatory effects of yeast and mammalian 14-3-3 proteins on the Raf protein kinase. *Science* 265:1716–1719.
7. Michaud NR, Fabian JR, Mathes KD, Morrison DK (1995) 14-3-3 is not essential for Raf-1 function: identification of Raf-1 proteins that are biologically activated in a 14-3-3- and Ras-independent manner. *Mol Cell Biol* 15:3390–3397.
8. Muslin AJ, Tanner JW, Allen PM, Shaw AS (1996) Interaction of 14-3-3 with signaling proteins is mediated by the recognition of phosphoserine. *Cell* 84:889–897.
9. Yaffe MB, et al. (1997) The structural basis for 14-3-3:phosphopeptide binding specificity. *Cell* 91:961–971.
10. Ganguly S, et al. (2005) Melatonin synthesis: 14-3-3-dependent activation and inhibition of arylalkylamine N-acetyltransferase mediated by phosphoserine-205. *Proc Natl Acad Sci USA* 102:1222–1227.
11. Coblitz B, Wu M, Shikano S, Li M (2006) C-terminal binding: an expanded repertoire and function of 14-3-3 proteins. *FEBS Lett* 580:1531–1535.
12. Pozuelo Rubio M, et al. (2004) 14-3-3-affinity purification of over 200 human phosphoproteins reveals new links to regulation of cellular metabolism, proliferation and trafficking. *Biochem J* 379:395–408.
13. Meek SE, Lane WS, Piwnica-Worms H (2004) Comprehensive proteomic analysis of interphase and mitotic 14-3-3-binding proteins. *J Biol Chem* 279:32046–32054.
14. Jin J, et al. (2004) Proteomic, functional, and domain-based analysis of in vivo 14-3-3 binding proteins involved in cytoskeletal regulation and cellular organization. *Curr Biol* 14:1436–1450.
15. Zippo A, et al. (2009) Histone crosstalk between H3S10ph and H4K16ac generates a histone code that mediates transcription elongation. *Cell* 138:1122–1136.
16. Masters SC, Fu H (2001) 14-3-3 proteins mediate an essential anti-apoptotic signal. *J Biol Chem* 276:45193–45200.
17. Petosa C, et al. (1998) 14-3-3zeta binds a phosphorylated Raf peptide and an unphosphorylated peptide via its conserved amphipathic groove. *J Biol Chem* 273:16305–16310.
18. Wang B, et al. (1999) Isolation of high-affinity peptide antagonists of 14-3-3 proteins by phage display. *Biochemistry* 38:12499–12504.
19. Du Y, Masters SC, Khuri FR, Fu H (2006) Monitoring 14-3-3 protein interactions with a homogeneous fluorescence polarization assay. *J Biomol Screen* 11:269–276.
20. Kim YC, et al. (1998) Synthesis and structure-activity relationships of pyridoxal-6-arylazo-5′ phosphate and phosphonate derivatives as P2 receptor antagonists. *Drug Develop Res* 45:52–66.
21. Fu H, Coburn J, Collier RJ (1993) The eukaryotic host factor that activates exoenzyme S of Pseudomonas aeruginosa is a member of the 14-3-3 protein family. *Proc Natl Acad Sci USA* 90:2320–2324.
22. Liu D, et al. (1995) Crystal structure of the zeta isoform of the 14-3-3 protein. *Nature* 376:191–194.
23. Obsil T, Ghirlando R, Klein DC, Ganguly S, Dyda F (2001) Crystal structure of the 14-3-3zeta:serotonin N-acetyltransferase complex. a role for scaffolding in enzyme regulation. *Cell* 105:257–267.
24. Yang X, et al. (2006) Structural basis for protein-protein interactions in the 14-3-3 protein family. *Proc Natl Acad Sci USA* 103:17237–17242.
25. Macdonald N, et al. (2005) Molecular basis for the recognition of phosphorylated and phosphoacetylated histone h3 by 14-3-3. *Mol Cell* 20:199–211.
26. Hoijemberg PA, Karlen SD, Sanrame CN, Aramendia PF, Garcia-Garibay MA (2009) Photolysis of an asymmetrically substituted diazene in solution and in the crystalline state. *Photochem Photobiol S* 8:961–969.
27. Subramanian RR, Masters SC, Zhang H, Fu H (2001) Functional conservation of 14-3-3 isoforms in inhibiting bad-induced apoptosis. *Exp Cell Res* 271:142–151.
28. Knight DA, Finck-Barbancon V, Kulich SM, Barbieri JT (1995) Functional domains of Pseudomonas aeruginosa exoenzyme S. *Infect Immun* 63:3182–3186.
29. Storoni LC, McCoy AJ, Read RJ (2004) Likelihood-enhanced fast rotation functions. *Acta Crystallogr D* 60:432–438.
30. Ottmann C, et al. (2007) Phosphorylation-independent interaction between 14-3-3 and exoenzyme S: from structure to pathogenesis. *Embo J* 26:902–913.
31. Emsley P, Cowtan K (2004) COOT: model-building tools for molecular graphics. *Acta Crystallogr D* 60:2126–2132.
32. Jones TA, Zou JY, Cowan SW, Kjeldgaard M (1991) Improved methods for building protein models in electron density maps and the location of errors in these models. *Acta Crystallogr A* 47:110–119.
33. Brunger AT, et al. (1998) Crystallography and NMR system: a new software suite for macromolecular structure determination. *Acta Crystallogr D* 54:905–921.
34. Schuttelkopf AW, van Aalten DM (2004) PRODRG: a tool for high-throughput crystallography of protein-ligand complexes. *Acta Crystallogr D* 60:1355–1363.
35. Annan RS, Carr SA (1996) Phosphopeptide analysis by matrix-assisted laser desorption time-of-flight mass spectrometry. *Anal Chem* 68:3413–3421.
36. Neubauer G, Mann M (1999) Mapping of phosphorylation sites of gel-isolated proteins by nanoelectrospray tandem mass spectrometry: potentials and limitations. *Anal Chem* 71:235–242.
37. Kinumi T, Niwa H, Matsumoto H (2000) Phosphopeptide sequencing by in-source decay spectrum in delayed extraction matrix-assisted laser desorption ionization time-of-flight mass spectrometry. *Anal Biochem* 277:177–186.
38. Jagannadham MV, Nagaraj R (2008) Detecting the site of phosphorylation in phosphopeptides without loss of phosphate group using MALDI TOF mass spectrometry. *Analytical Chemistry Insights* 3:21–29.